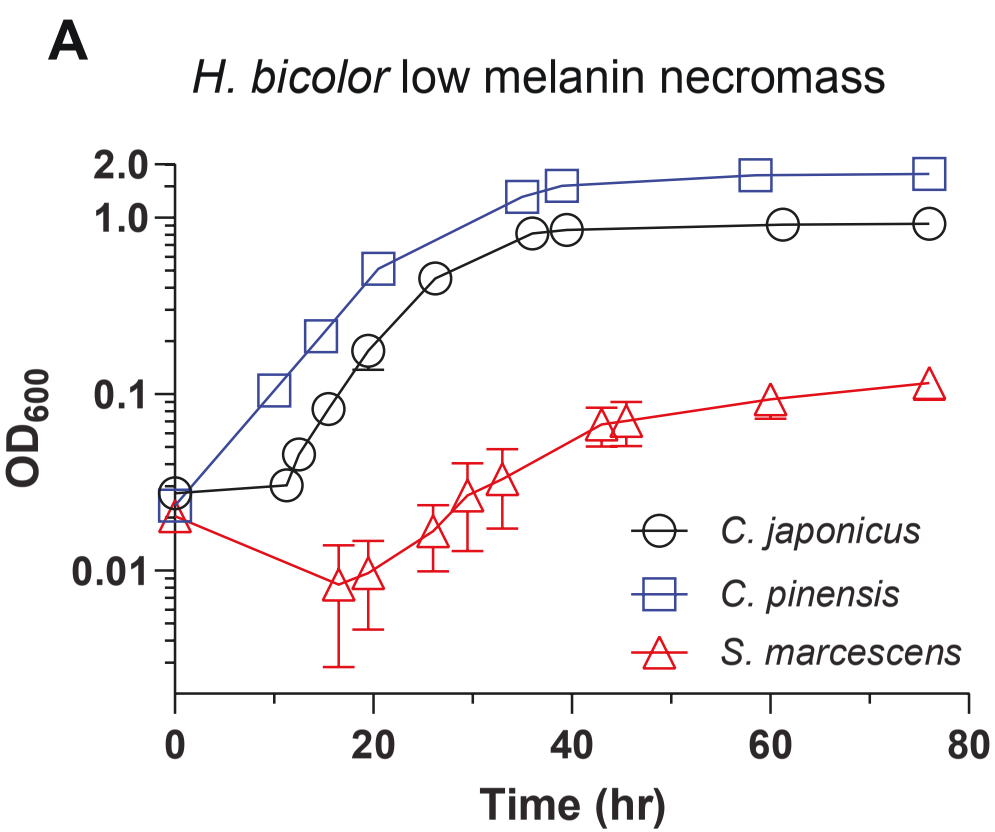
A
H. bicolor low melanin necromass
2.0
1.0
0.1
0.01
OD600
0
20
40
60
80
Time (hr)
C. japonicus
C. pinensis
S. marcescens

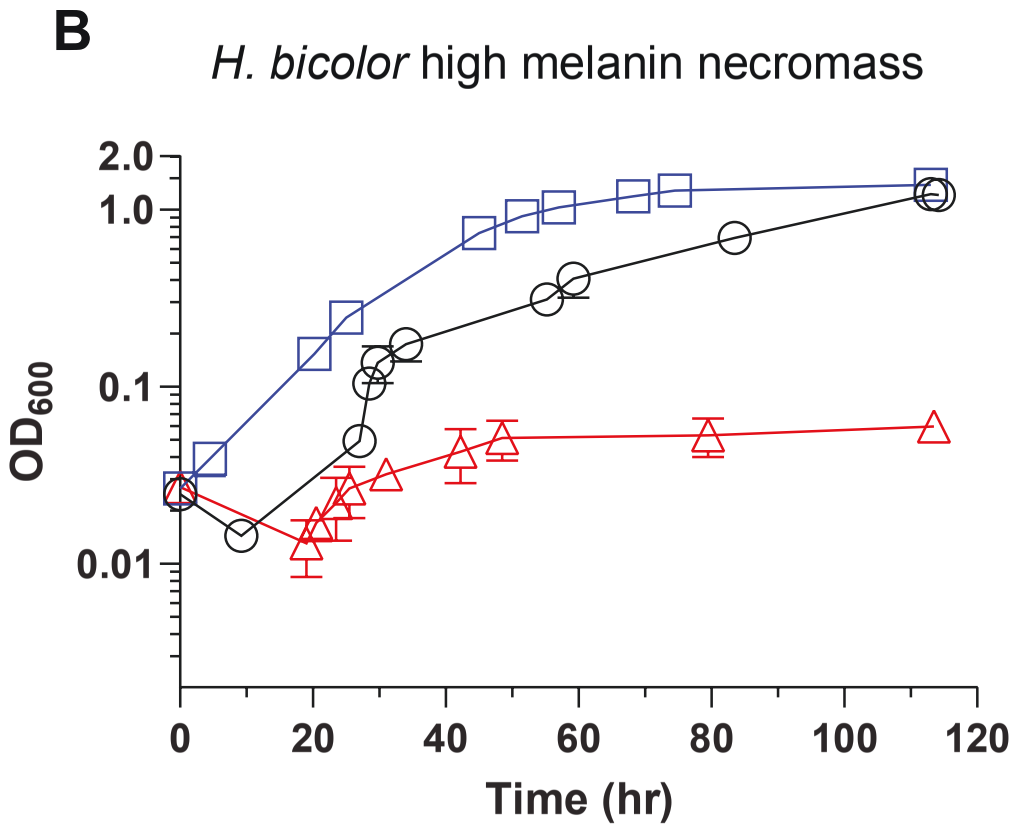
B
H. bicolor high melanin necromass
2.0
1.0
0.1
0.01
OD600
0
20
40
60
80
100
120
Time (hr)

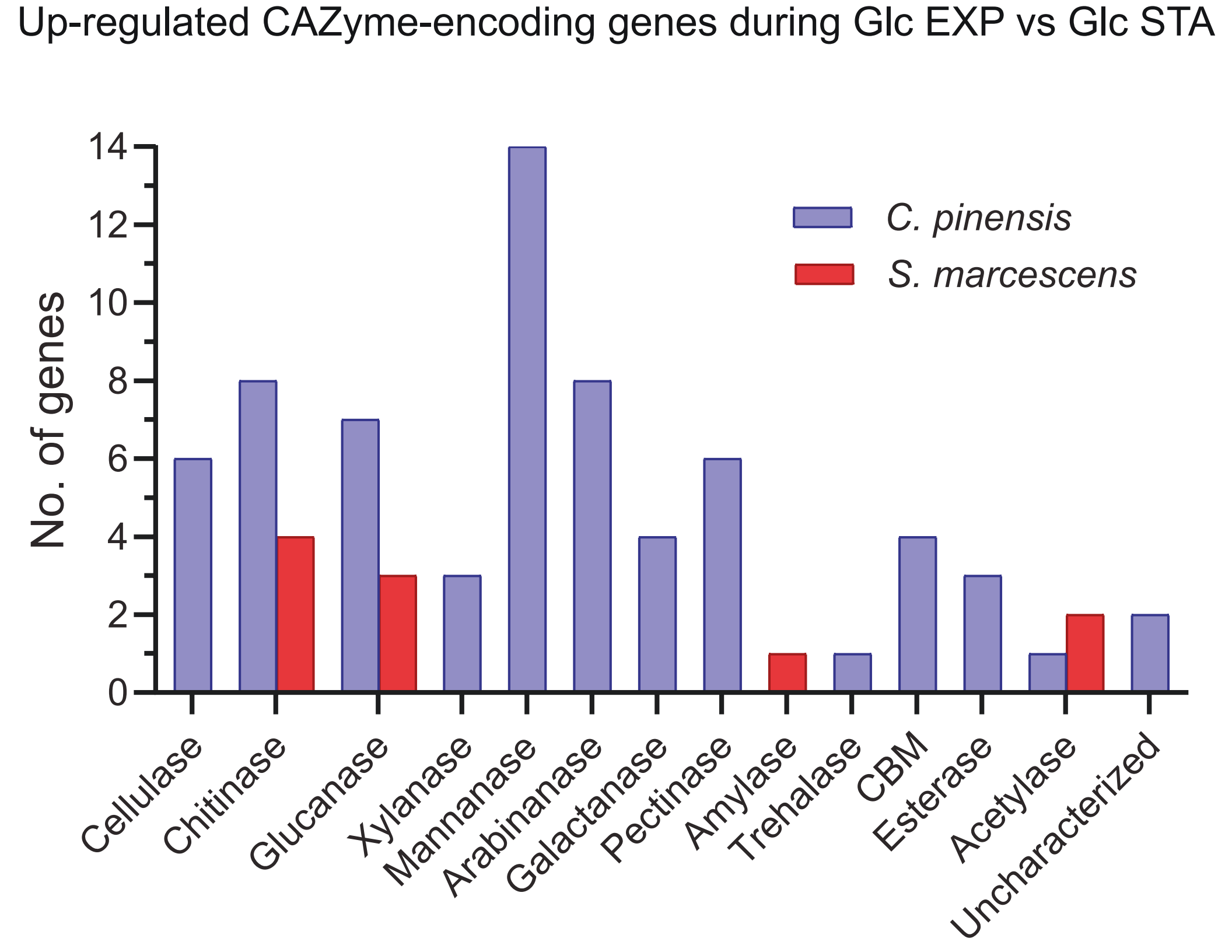
Up-regulated CAZyme-encoding genes during Glc EXP vs Glc STA
No. of genes
0
2
4
6
8
10
12
14
C. pinensis
S. marcescens
Cellulase
Chitinase
Glucanase
Xylanase
Mannanase
Arabinanase
Galactanase
Pectinase
Amylase
Trehalase
CBM
Esterase
Acetylase
Uncharacterized

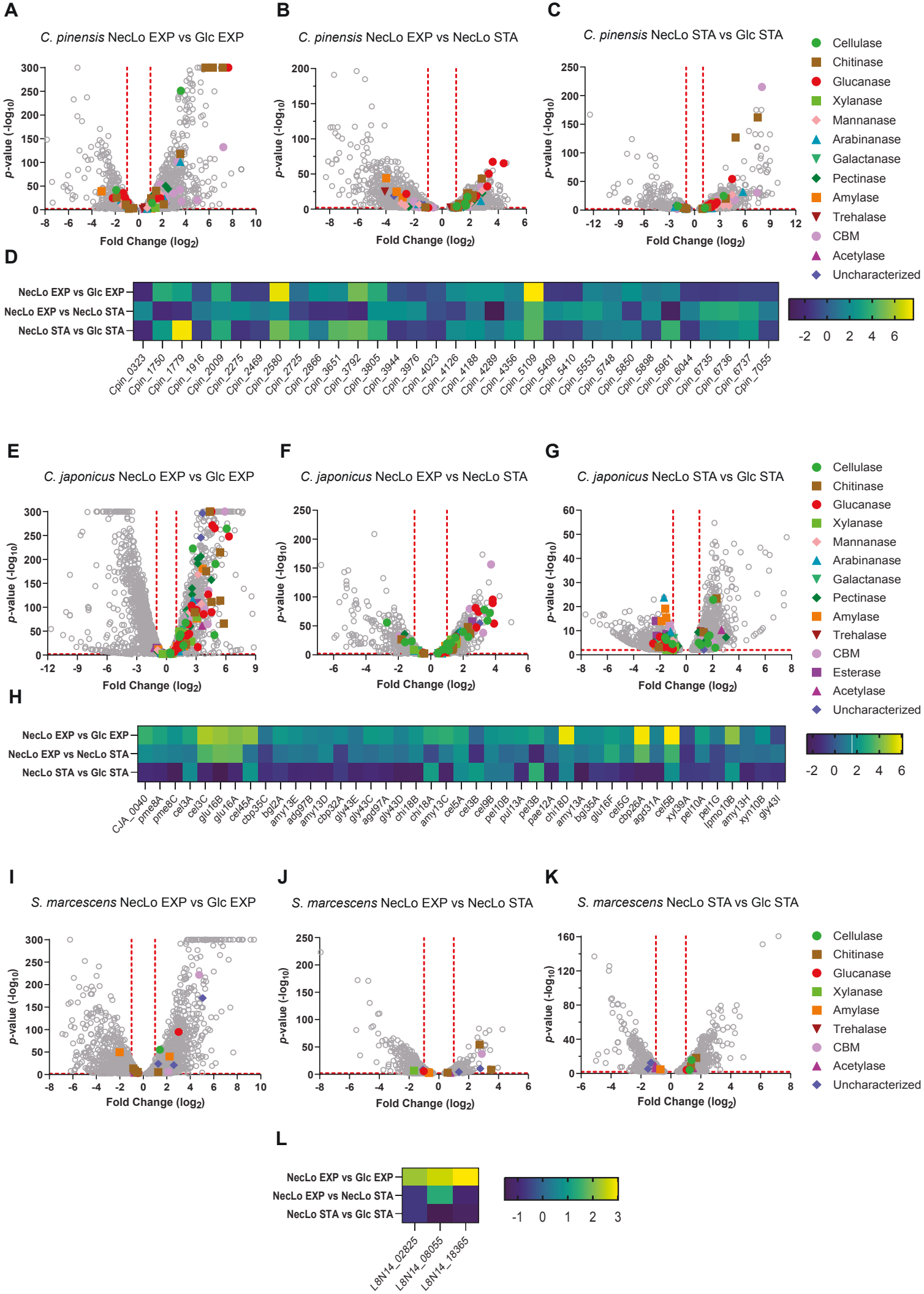
A
C. pinensis NecLo EXP vs Glc EXP
B
C. pinensis NecLo EXP vs NecLo STA
C
C. pinensis NecLo STA vs Glc STA
p-value (-log10)
Fold Change (log2)
Cellulase
Chitinase
Glucanase
Xylanase
Mannanase
Arabinanase
Galactanase
Pectinase
Amylase
Trehalase
CBM
Acetylase
Uncharacterized
D
NecLo EXP vs Glc EXP
NecLo EXP vs NecLo STA
NecLo STA vs Glc STA
Cpin_0323 Cpin_1750 Cpin_1779 Cpin_1916 Cpin_2009 Cpin_2275 Cpin_2469 Cpin_2580 Cpin_2725 Cpin_2866 Cpin_3651 Cpin_3792 Cpin_3805 Cpin_3944 Cpin_3976 Cpin_4023 Cpin_4126 Cpin_4188 Cpin_4289 Cpin_4356 Cpin_5109 Cpin_5409 Cpin_5410 Cpin_5553 Cpin_5748 Cpin_5850 Cpin_5898 Cpin_5961 Cpin_6044 Cpin_6735 Cpin_6736 Cpin_6737 Cpin_7055
-2 0 2 4 6
E
C. japonicus NecLo EXP vs Glc EXP
F
C. japonicus NecLo EXP vs NecLo STA
G
C. japonicus NecLo STA vs Glc STA
Cellulase
Chitinase
Glucanase
Xylanase
Mannanase
Arabinanase
Galactanase
Pectinase
Amylase
Trehalase
CBM
Esterase
Acetylase
Uncharacterized
H
NecLo EXP vs Glc EXP
NecLo EXP vs NecLo STA
NecLo STA vs Glc STA
CJA_0040 pme8A pme8C cel3A cel3C glu16B glu16A cel45A cbp35C bgl2A amy13E agd97B amy13D cbp32A gly43E gly43C agd97A gly43D chi18B chi18A amy13C cel5A cel3B cel9B pel10B pul13A pel3B pae12A chi18D amy13A bgl35A glu16F cel5G cbp26A agd31A cel5B xyl39A pel10A pel1G lpmo10B amy13H xyn10B gly43I
-2 0 2 4 6
I
S. marcescens NecLo EXP vs Glc EXP
J
S. marcescens NecLo EXP vs NecLo STA
K
S. marcescens NecLo STA vs Glc STA
Cellulase
Chitinase
Glucanase
Xylanase
Amylase
Trehalase
CBM
Acetylase
Uncharacterized
L
NecLo EXP vs Glc EXP
NecLo EXP vs NecLo STA
NecLo STA vs Glc STA
L8N14_02825 L8N14_08055 L8N14_18365
-1 0 1 2 3

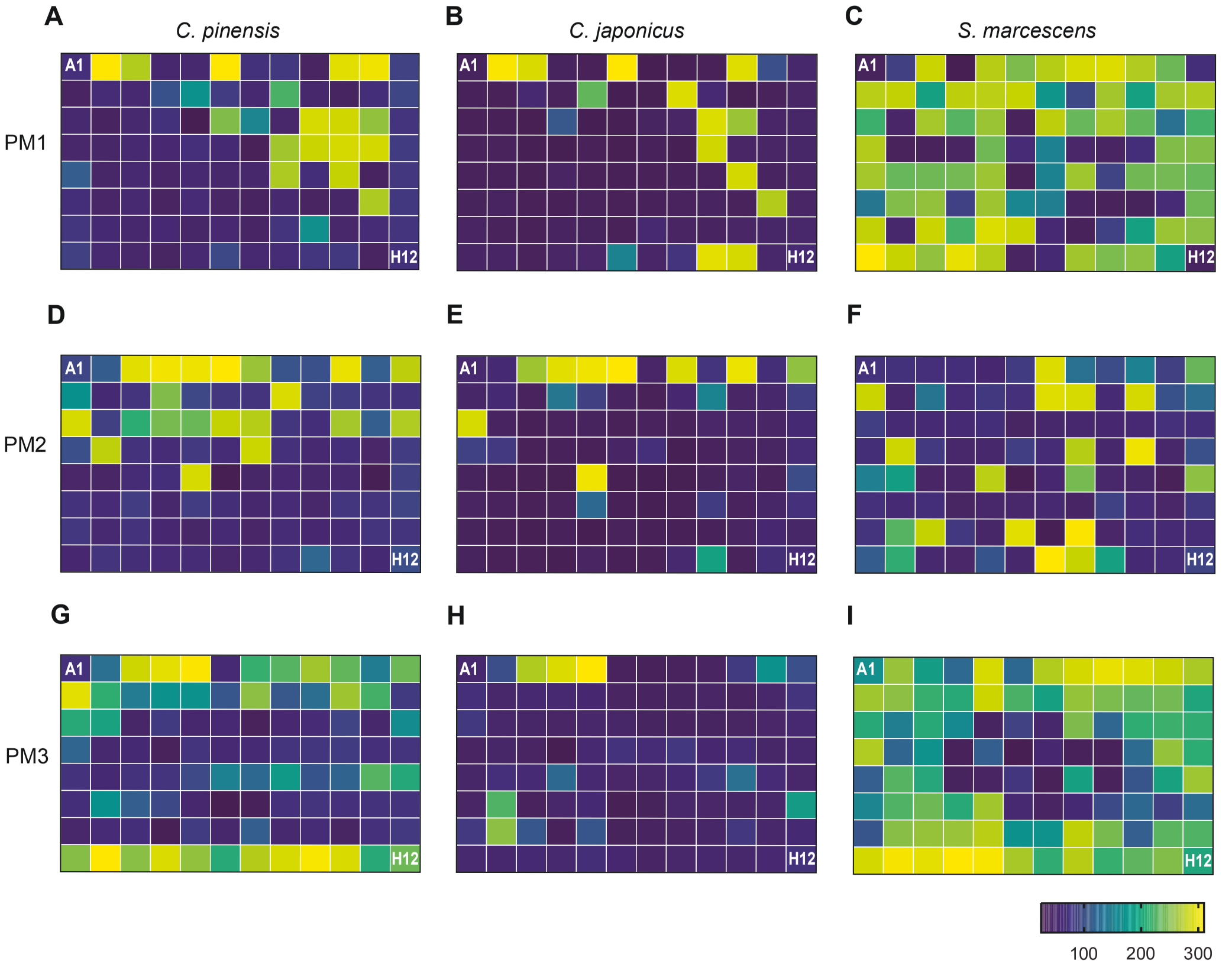
A
C. pinensis
B
C. japonicus
C
S. marcescens
PM1
PM2
PM3
D
E
F
G
H
I
A1
H12
100
200
300

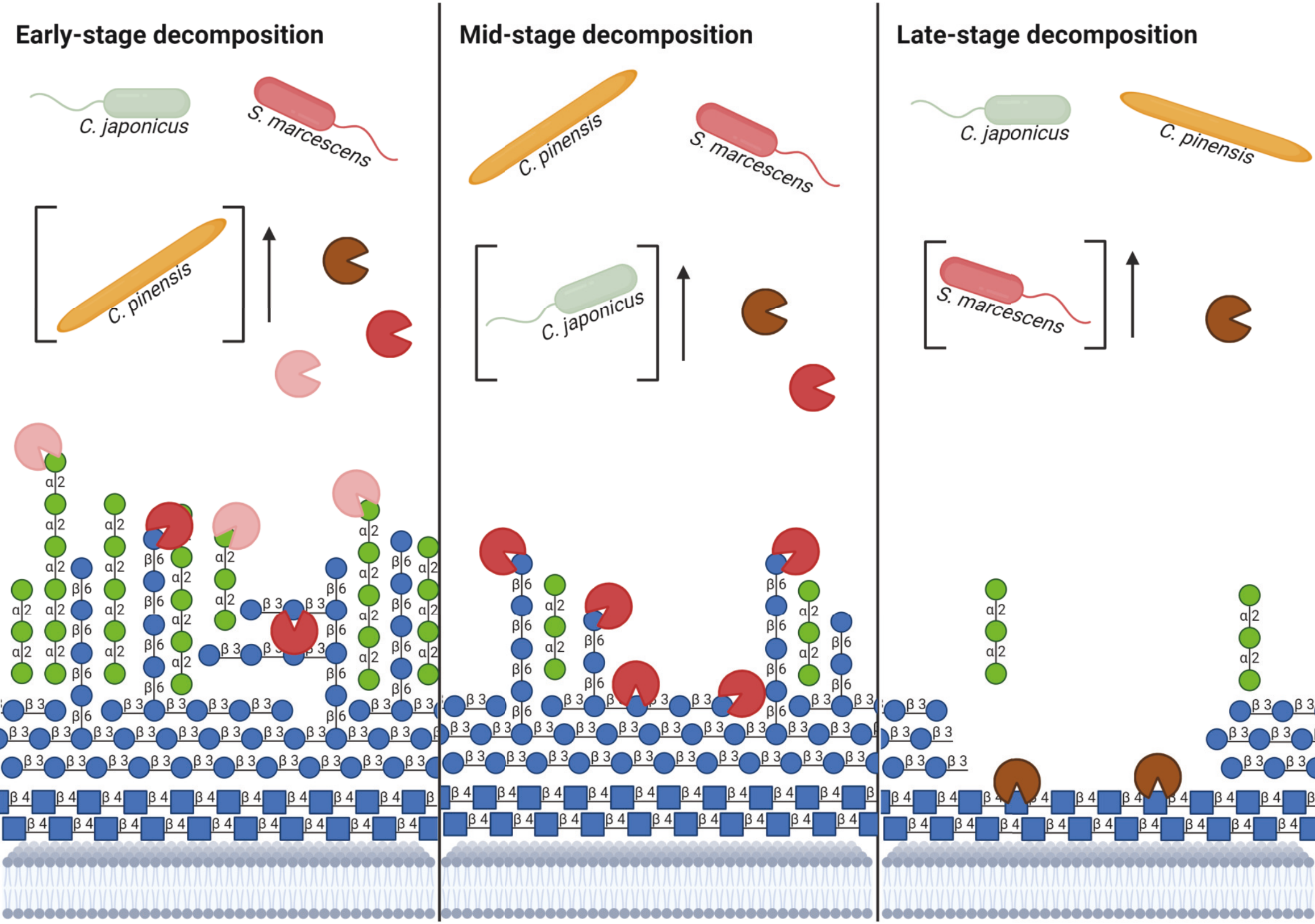
Early-stage decomposition
C. japonicus
S. marcescens
C. pinensis
Mid-stage decomposition
C. pinensis
S. marcescens
C. japonicus
Late-stage decomposition
C. japonicus
C. pinensis
S. marcescens

Transcriptomic analyses of bacterial growth on fungal necromass reveals different microbial community niches during degradation

Jessica K. Novak[1], Peter G. Kennedy[2], and Jeffrey G. Gardner[1#]

Running Title
Transcriptomic analysis of bacteria grown on fungal necromass

Keywords
Carbohydrate active enzyme, *Cellvibrio japonicus*, *Chitinophaga pinensis*, *Hyaloscypha bicolor*, necromass, *Serratia marcescens*

Author Affiliations
[1]Department of Biological Sciences, University of Maryland - Baltimore County Baltimore, Maryland, USA

[2]Department of Plant and Microbial Biology, University of Minnesota, Minneapolis, Minnesota, USA

[#]Correspondence
Jeffrey G. Gardner
Department of Biological Sciences
University of Maryland - Baltimore County
Email: jgardner@umbc.edu
Phone: 410-455-3613
Fax: 410-455-3875

ABSTRACT

Bacteria are major drivers of organic matter decomposition and play crucial roles in global nutrient cycling. Although the degradation of dead fungal biomass (necromass) is increasingly recognized as an important contributor to soil carbon (C) and nitrogen (N) cycling, the genes and metabolic pathways involved in necromass degradation are under characterized. In particular, how bacteria degrade necromass containing different quantities of melanin, which largely control rates of necromass decomposition *in situ*, is largely unknown. To address this gap, we conducted a multi-timepoint transcriptomic analysis using three Gram-negative, bacterial species grown on low or high melanin necromass of *Hyaloscypha bicolor.* The bacterial species, *Cellvibrio japonicus, Chitinophaga pinensis*, and *Serratia marcescens*, belong to genera known to degrade necromass *in situ.* We found that while bacterial growth was consistently higher on low than high melanin necromass, the CAZyme-encoding gene expression response of the three species was similar between the two necromass types. Interestingly, this trend was not shared for genes encoding nitrogen utilization, which varied in *C. pinensis* and *S. marcescens* during growth on high versus low melanin necromass. Additionally, this study tested the metabolic capabilities of these bacterial species to grow on a diversity of C and N sources and found that the three bacteria have substantially different utilization patterns. Collectively, our data suggests that as necromass changes chemically over the course of degradation, certain bacterial species are favored based on their differential metabolic capacities.

IMPORTANCE

Fungal necromass is a major component of the carbon (C) in soils as well as an important source of nitrogen (N) for plant and microbial growth. Bacteria associated with necromass represent a distinct subset of the soil microbiome and characterizing their functional capacities is the critical next step toward understanding how they influence necromass turnover. This is particularly important for necromass varying in melanin content, which has been observed to control the rate of necromass decomposition across a variety of ecosystems. Here we assessed gene expression of three necromass-degrading bacteria grown on low or high melanin necromass and characterized their metabolic capacities to grow on different C and N substrates. These transcriptomic and metabolic studies provide the first steps towards assessing the physiological relevance of up-regulated CAZyme-encoding genes in necromass decomposition and provide foundational data for generating a predictive model of the molecular mechanisms underpinning necromass decomposition by soil bacteria.

INTRODUCTION

Ectomycorrhizal (ECM) fungi are major drivers of soil nutrient cycling in forest ecosystems worldwide (1–3). Through their extensive mycelial networks and diverse enzymatic capacities, ECM fungi scavenge nutrients from sources and spaces in soil that are largely inaccessible to plants (4,5). These nutrients are then traded with plant hosts in exchange for photosynthetically derived sugars (6). This interaction ends with the death of either the plant or the ECM fungus, and the resulting organic material enters the brown food web as a substrate for decomposition. While carbon utilization and nutrient recovery from dead plant material by soil microbes is well characterized, much less known about microbial resource acquisition derived from dead ECM fungi (7, 8) despite previous knowledge that fungal necromass decomposition can be a significant contributor to soil carbon and nutrient cycling (9,10).

It is hypothesized that fungal cell wall components are the major sources of carbon and nutrition available in necromass (11). The carbohydrate component of necromass includes β-glucans, α-chitin, and α-mannans, and these substrates possess β-1,3- and β-1,6-linked glucose, β-1,4-linked *N*-acetylglucosamine, and α-1,2-linked mannose, respectively (12). In terms of fungal cell wall structure, the outermost layer is often the thickest and largely comprised of α-mannans and β-glucans, with α-chitin deeper within the cell wall and closer to the membrane (13). Necromass also frequently contains melanin (14) which is a complex polymer derived from 3,4-dihydroxyphenylalanine (DOPA) that is intermeshed amongst the polysaccharides of the fungal cell wall (15–17). Notably, previous studies on fungal cell wall degradation found that a high melanin

content slowed the decomposition rate because it limited access to polysaccharides and/or disrupted the membrane of the microbial decomposers (18, 19).

In this study, we used the necromass of *Hyaloscypha bicolor,* formerly known as *Meliniomyces bicolor* (20). The rationale of using this fungus is that it can be naturally manipulated to have either low or high melanin phenotypes (21), which have been consistently demonstrated to have different rates of decay (22,23). Previous work on *H. bicolor* degradation by bacterial decomposers found changes in the necrobiome community based on melanin content, stage of decay, and the associated plant host (21). The dominating bacterial decomposers included genera such as *Chitinophaga, Pseudomonas, Cellvibrio, Burkholderia,* and *Luteibacter* (21). However, identifying the contribution of individual bacterial genera to fungal cell wall degradation has been understudied (24). Consequently, there is a need to investigate the saccharifying capabilities of necromass-degrading bacteria to assemble a working model of *H. bicolor* decomposition that includes in both spatial and temporal aspects.

To begin our study, we measured the growth and gene expression of three bacterial species using both high and low melanin phenotypes of *H. bicolor* necromass. The bacterial species (*Cellvibrio japonicus* Ueda107*, Chitinophaga pinensis* DSM2588*,* and *Serratia marcescens* PIC3611) were selected because they are proficient polysaccharide degraders, and members of these three genera have been previously identified as being associated with decaying necromass in situ (21). Another shared characteristic of these genera is their expansive suite of carbohydrate-active enzymes (CAZymes), which are able to hydrolyze the diverse glycosidic linkages found in fungal cell wall polysaccharides (25–28). Examples of CAZymes required for fungal cell wall

129 degradation include glycoside hydrolases (GHs), lytic polysaccharides monooxygenases
130 (LPMOs), and carbohydrate esterases (CEs) (29–31).

131 By assessing the gene expression of each bacterial species grown on *H. bicolor*
132 necromass, we identified CAZyme-encoding gene targets with likely physiological
133 importance for necromass decomposition. Additionally, comparing the growth dynamics
134 and expression responses of the three bacterial species on high versus low melanin *H.*
135 *bicolor* necromass helped to explain the decelerated decay rate of high melanin
136 necromass. In terms of growth capabilities, we found that the bacterial growth rates were
137 generally slower on high melanin necromass and often resulted in a lower final cell
138 density. However, the CAZyme-encoding gene expression responses were almost
139 identical for all three species on both the high and low melanin necromass. This gene
140 expression analyses also revealed that *C. pinensis* gene expression was regulated both
141 temporally and by substrate, whereas *C. japonicus* and *S. marcescens* CAZyme gene
142 expression were largely regulated by substrate. Further, we performed a phenotypic
143 microarray to identify substrate utilization for each bacterial species on 190 carbon
144 sources and 95 nitrogen sources and found that *S. marcescens* is metabolically active on
145 a much broader array of sole nitrogen sources compared to the other two strains. Overall,
146 our results identified distinct bioconversion differences among the bacterial species,
147 which aided in the generation of a model for necromass degradation by bacteria.

148

149 **METHODS**

150 ***Necromass preparation.*** *Hyaloscypha bicolor* (formerly *Meliniomyces bicolor*) cultures
151 were grown on half-strength potato dextrose (PD; HiMedia Laboratories, PA, USA) agar

plates covered with gel drying film (Promega, WI, USA). *H. bicolor* cultures were maintained at 23 ^{O}C in the dark for three weeks. Mycelial plugs were transferred to liquid PD broth with pH adjusted to 5 using 10% HCl. Cultures were grown in 125 mL flasks filled with either 40 or 110 mL for low and high melanin biomass, respectively. The cultures were then grown in shaking incubators (120 RPM for low melanin and 150 RPM for high melanin) for 30 days at 25 ^{O}C. *H. bicolor* mycelium were then harvested in bulk onto sterile sieves and rinsed with sterile deionized water. Next, the mycelium of each melanization level was homogenized using a sterilized mortar and pestle, transferred to sterile 50 mL centrifuge tubes (Fisherbrand, PA, USA), and stored at -80ºC overnight. Tubes were then placed into a benchtop Freeze Dryer (Labconco, NH, USA) for three days at -50ºC under vacuum to create the necromass used in this study.

Bacterial Growth Conditions. *C. japonicus* Ueda107*, C. pinensis* DSM2588*,* and *S. marcescens* PIC3611 strains were grown in MOPS defined media (TekNova #M2106), supplemented with 1.3 mM phosphate and 0.2% (w/v) glucose per manufacturer's instructions. Strains propagated in liquid culture were grown at 30 ^{O}C with high aeration (200 RPM) as done previously (32). Plate media was solidified with 1.5% (w/v) agar. Strains used for growth analyses were grown overnight in 5 mL MOPS-glucose broth until full density was reached (OD_{600} ~1.5), then diluted 1:100 into MOPS defined media containing 1.3 mM phosphate and either high or low melanin necromass at a concentration of 1% (w/v). The insoluble necromass was contained in 90 µm nylon mesh bags (The Press Club #B079S6JNQW). The necromass was autoclaved in deionized

water (30 min. steam cycle; 121 ^{O}C, 16psi), and then rinsed twice with sterile deionized water before use in growth experiments.

Transcriptome Sampling and Analysis. Transcriptome sampling was conducted as previously described (32). Briefly, cultures were grown in 500 mL flasks in biological triplicate with MOPS defined media and either 0.2% (w/v) glucose or 1% (w/v) necromass. Optical density (OD_{600}) measurements were taken to capture the growth dynamics of the three bacterial species on each substrate over four days. Sampling occurred during mid-exponential growth and stationary phase, where cultures that reached mid-exponential growth at $OD_{600} \geq 0.1$, then 35 mL of culture was aseptically collected and added to 5 mL phenol:ethanol (5:95; v/v) to stop metabolism. In cultures with mid-exponential growth $OD_{600} \leq 0.1$, 70 mL of culture as added to a 10 mL phenol:ethanol (5:95 v/v) to ensure sufficient cell mass was obtained. The metabolically stopped cell suspensions were then immediately centrifuged at 8000 x g for 5 min. at 4 ^{O}C. Supernatants were removed, and cell pellet was flash-frozen in a dry ice and ethanol bath for 5 minutes before storage in -80 ^{O}C. Frozen cell pellets were sent to Azenta (South Plainfield, NJ) for mRNA extraction, mRNA QA, cDNA library preparation, and RNAseq. All samples had a RIN above 8.0 during QA. Sequencing used an Illumina HiSeq and generated ~350M pair-end (2x150bp), single index reads, and ~90% of bases >Q30 with mean quality score >35. The raw FASTQ files were quality checked, aligned to existing genomes, and analyzed for differential expression using the Galaxy platform (33). Unless otherwise noted below, default parameters were in all analysis tools used except in cases where strandedness was specified (all RNAseq data were unstranded). Briefly, RNAseq data were

197 concatenated using the concatenate data sets: tail-to-head (cat) tool (34). Transcript
198 quality was tested using FastQC, which indicated read trimming was unnecessary for any
199 of the files (35). Transcripts were next aligned to their respective reference genomes
200 using the HISAT2 tool (36) and quantified using the htseq-count tool (37). Reference
201 genome files for *C. japonicus* Ueda107 (ASM1922v1) and *C. pinensis* DSM2588
202 (ASM2400v1) were obtained from ENSEMBLE, while that for *S. marcescens* PIC3611
203 was retrieved from NCBI Refseq (ASM2260299v1). Due to the differences in reference
204 genome sources, the *S. marcescens* files required a parameter change in the htseq-count
205 'feature type' from 'gene' to 'exon'. Differential gene expression using DESeq2 compared
206 exponential growth of the experimental condition (either high or low melanin necromass)
207 to that of glucose exponential growth, necromass stationary phase to that of glucose
208 stationary phase, and necromass exponential growth to necromass stationary phase (38).
209 All RNAseq data have been deposited in NCBI GEO (BioProjects GSE149593 and
210 GSE268149). The RNAseq data for *C. japonicus* grown on glucose was obtained from
211 NCBI SRA: SRX8207642, SRX8207643, SRX8207644, SRX8207645, SRX8207646, and
212 SRX8207647. Glucose RNAseq data for *C. pinensis* and *S. marcescens* have been
213 deposited in NCBI SRA (*C. pinensis* SRX24655130, SRX24655128, SRX24655127,
214 SRX24655125, SRX24655124, and SRX24655122; *S. marcescens* SRX24655148,
215 SRX24655147, SRX24655146, SRX24655145, SRX24655144, and SRX24655143).
216 High melanin *H. bicolor* RNAseq data have been deposited in NCBI SRA (*C. japonicus*
217 SRX24655114, SRX24655113, SRX24655112, SRX24655111, SRX24655109, and
218 SRX24655107; *C. pinensis* SRX24655136, SRX24655135, SRX24655134,
219 SRX24655133, SRX24655132, and SRX24655131; *S. marcescens* SRX24655154,

SRX24655153, SRX24655152, SRX24655151, SRX24655150, and SRX24655149). Low melanin *H. bicolor* RNAseq data have been deposited in NCBI SRA (*C. japonicus* SRX24655120, SRX24655119, SRX24655118, SRX24655117, SRX24655116, and SRX24655115; *C. pinensis* SRX24655142, SRX24655141, SRX24655140, SRX24655139, SRX24655138, and SRX24655137; *S. marcescens* SRX24655160, SRX24655159, SRX24655158, SRX24655157, SRX24655156, and SRX24655155).

Phenotypic Microarray Assay. Carbon and nitrogen utilization assays were completed by BioLog (Newark, DE) on a fee-for-service basis. Experiments were performed in biological triplicate in MOPS defined media at 30 ^{O}C for 24 hours in a 96-well assay plate format using methods similar to those previously published (39, 40). A comprehensive list of all carbon and nitrogen sources tested can be found in **Tables S24 – S26**.

Thermochemolysis-gas chromatography-mass spectrometry. *H. bicolor* necromass with an intermediate level of melaninization underwent thermochemolysis-GCMS (pyGCMS) to assess its biological makeup as previously described (23). Briefly, ca. 15 ml of tetramethylammonium hydroxide (TMAH) was added to 140-150 micrograms of ground and dried necromass. Samples were heated to 300 ^{O}C at a rate of 720 ^{O}C/min in a Gerstel Thermal Desorption Unit and immediately introduced into the GC column (HP-5MS, 30 m x 0.250 mm, 0.25 mm film thickness). The GC-oven (Agilent Technologies, 7890B, Santa Clara, CA, USA) was heated from 50 ^{O}C to 320 ^{O}C over 55 min and held at 320 ^{O}C for 10 min. Molecules were ionized in an Agilent Technologies 5977A mass spectrometer by electron ionization with a voltage of 70 eV. The generated peaks were

classified as either aromatics, carbohydrates, lipids, nitrogen-containing, sterols, or compounds of unspecified origin by their mass spectra using Agilent ChemStation software (standard runs) and the NIST library. The N-containing fragments included proteins and amino sugars and therefore include N-containing chitin fragments. Single ion monitoring (SIM) was performed by Agilent MassHunter software and the relative abundances of each compound was calculated using a MATLAB script.

RESULTS

GROWTH ANALYSES

The three bacterial species were first grown on glucose, where minor growth variances were observed (**Fig. S1 & Table S1**). *C. japonicus* had the fastest growth rate, shortest lag phase, and highest final cell density when provided glucose as the sole carbon source. Alternatively, *C. pinensis* and *S. marcescens* shared similar growth rates, with the former reaching a higher final cell density.

All three species were next grown on high and low melanin necromass to assess the growth variances between the two substrates and relative to a glucose growth baseline. *C. pinensis* had the shortest lag phase among the three species when growing on necromass (**Fig. 1, Table S2**), but the precise length of time in lag phase could not be determined for *C. pinensis* on low melanin necromass due to its fast growth and gaps in sampling due to the design for protracted growth experiments. *C. pinensis* also had the highest final cell density on low melanin necromass and shared the highest final cell density on high melanin necromass compared to *S. marcescens* and *C. japonicus.* In a comparison of the growth dynamics on both necromass types, *C. pinensis* grew nearly twice as fast on the low than high melanin necromass and reached a higher cell density.

C. japonicus had a relatively consistent growth rate on low melanin necromass compared to high melanin necromass (**Fig. 1, Table S2**). Intriguingly, the growth dynamics of *C. japonicus* on high melanin necromass had several irregular phases of growth. Specifically, the exponential growth phase was rapid and only spanned roughly 5 hours (OD_{600} 0.03 – 0.2), while the transition into stationary phase lasted roughly 75 hours (OD_{600} 0.2 – 1.0). Furthermore, stationary phase was reached much sooner on the

low melanin necromass at 40 hours as opposed to the 100+ hours on high melanin necromass.

Of the three species, *S. marcescens* exhibited the poorest growth on both necromass types, with comparatively very low final cell densities (**Fig. 1, Table S2**). However, growth of *S. marcescens* on low melanin necromass had a final cell density that was double the final cell density on high melanin necromass. *S. marcescens* also maintained exponential growth on low melanin necromass for twice the time compared to high melanin necromass, albeit with a slower growth rate.

TRANSCRIPTOMIC ANALYSES – CARBON AND NITROGEN UTILIZATION

Baseline gene expression profiles using glucose. Before conducting gene expression analyses for all three species on necromass, we identified genes with growth rate-controlled expression by comparing the RNAseq data of each strain grown on glucose during exponential growth compared to stationary phase. Stationary phase was used as the reference condition for this analysis to maintain focus on the response of metabolically active cells. Since this type of analysis has already been reported in *C. japonicus* (41, 42), our assessment initially focused on *C. pinensis* and *S. marcescens.* The comparative expression data is reported here as “Substrate GrowthPhase vs Substrate GrowthPhase” (*e.g.* Glc EXP vs Glc STA). These abbreviations indicate that the gene expression data are reflective of the former condition (*e.g.* Glc EXP) when compared to the latter condition (*e.g.* Glc STA). The supplementary tables containing differential gene expression data were filtered to only include the expression values when the *p*-value was significant at a level of $\leq$ 0.01. Therefore, genes that are absent from some tables (but not others) are

due to removal because of a non-significant *p*-value. Predicted activity of CAZyme-encoding genes in *C. pinensis* DSM2588 were determined based on the annotated genome from EnsemblBacteria and previous proteomic studies (43). The predicted CAZyme-encoding genes for *S. marcescens* PIC3611 were determined by the annotated genome from NCBI (44). In total, *C. pinensis* has 357 CAZyme-encoding genes, while *S. marcescens* has 113.

In *C. pinensis*, comparison of the gene expression response on glucose during exponential growth compared to stationary phase showed up-regulation of more than 2,000 genes (27% of the genome). The top 50 up-regulated genes predominantly encoded proteins with functions in nutrient acquisition. This included genes which encode a variety of predicted functions such as transport, carbohydrate binding, glycoside hydrolysis, and nitrogen metabolism (**Table S3**). In terms of nitrogen utilization, the up-regulated genes encoded a glutamate-ammonia ligase (*cpin_7211*), glutamate synthetase (*cpin_1662*), threonine dehydratase (*cpin_1924*), histidine ammonia-lyase (*cpin_1853*) and two glutamate synthases (*cpin_0731* and *cpin_0730*). Additionally, among the up-regulated genes were 67 predicted CAZyme-encoding genes (19% of total in genome). While all the listed CAZyme-encoding genes for *C. pinensis* are computationally predicted, not all have experimentally confirmed activities. The predicted gene products were diverse in putative activity and included mannanases, chitinases, arabinanases, cellulases, and pectinases (**Fig. 2**). The predicted CAZyme-encoding genes that exhibited the highest fold-change in expression during exponential growth (among the top 50 up regulated genes; $\geq$ 3.5-fold $\log_2$) were three glucanase-encoding genes (*cpin_6735, cpin_6736,* and *cpin_6737*), one chitinase-encoding gene

(*cpin_5260*), and one α-mannanase-encoding gene (*cpin_4822*). The three glucanase-encoding genes are part of a predicted polysaccharide utilization locus (PUL) wherein *cpin_6737* has a four base-pair overlap with *cpin_6736,* and *cpin_6735* is 22 base pairs down-stream from *cpin_6736* (45). Additionally, *cpin_4822* is predicted to be part of a different PUL, however the neighboring α-mannanase-encoding gene (*cpin_4820*) was far less expressed.

In *S. marcescens,* a comparison between growth phases on glucose elicited up-regulation of more than 1,400 genes (26% of the genome). Among the top 50 up-regulated genes were products that largely confer motility, transport, and response regulation (**Table S4**). In terms of nitrogen utilization, *S. marcescens* elicited up-regulation of seven genes during exponential growth on glucose. The genes and their predicted products included the small subunit of nitrite reductase (*L8N14_21965*), a nitrogen regulation protein NR(I) (*L8N14_23630*), glutamine synthetase (*L8N14_12535*), glutamine amidotransferase (*L8N14_00130*), carbon-nitrogen hydrolase (*L8N14_05810*), aspartate ammonia-lyase (*L8N14_17335*), and threonine ammonia-lyase (*L8N14_21270*). During growth on glucose *S. marcescens* up-regulated few computationally predicted CAZyme-encoding genes. Only ten differentially expressed CAZyme-encoding genes (9% of total in genome) were identified, and included glucanases, chitinases, carbohydrate deacetylases, and an amylase (**Fig. 2**). The most up-regulated CAZyme-encoding genes (among the top 50 up-regulated genes; > 2-fold $\log_2$) encoded a polysaccharide deacetylase, two chitinases, phospho-β-glucosidase, and polysaccharide deacetylase with 3.2-, 3.1-, 2.7-, 2.4-, and 2.0-fold expression change ($\log_2$), respectively.

While *C. japonicus* analysis of CAZyme-encoding gene expression during exponential growth using glucose versus stationary phase was previously conducted, the up-regulated nitrogen utilization-encoding genes were not discussed. Our analysis of those previously published data identified the up-regulation of six nitrogen utilization-encoding genes that included glutamate dehydrogenase (*gdhA*), glutamine synthetase (*glnA*), glutamate synthase (*gltD*), threonine-ammonia lyase (*ilvA*), glutamine-dependent NAD+ synthetase (*adgA*), and nitroreductase (*cja_1559*).

CAZyme gene expression during growth on high and low melanin necromass. As a complement to the growth analyses, we conducted a transcriptomic study to better characterize bacterial *H. bicolor* decomposition. All RNAseq data underwent differential gene expression analysis using comparisons to glucose or opposing growth phases to identify physiologically relevant CAZyme-encoding genes, an approach that has been done previously (15, 16). The primary observation made from these results was that CAZyme-encoding gene expression for all three bacteria was almost identical for both types of necromass (**Tables S5 – S22**). Given that low melanin necromass possesses greater proportions of carbohydrates than high melanin necromass (23), below we report the results for CAZyme-encoding gene expression only for that necromass type. However, graphical representations of CAZyme-encoding gene expression for each species on high melanin necromass are presented in **Fig. S2**. Notably, several of the discussed CAZyme-encoding genes are only computationally predicted and not yet biochemically confirmed. CAZyme-encoding genes that are described as

364 “uncharacterized” are therefore predicted hydrolases that have not been classified into a
365 specific family of glycoside hydrolase or esterase.
366
367 ***C. pinensis CAZyme-encoding gene expression is regulated both temporally***
368 ***(exponential v. stationary phase) and by substrate (necromass v. glucose).*** Our *C.*
369 *pinensis* transcriptome analysis during growth on glucose in exponential growth
370 compared to stationary phase found that 33% of *C. pinensis* CAZyme-encoding genes
371 were regulated temporally. Comparison of the transcriptomic data for exponential growth
372 on low melanin necromass compared to glucose (NecLo EXP vs Glc EXP) also identified
373 CAZyme-encoding genes with substrate-induced expression. This latter comparison
374 identified 1,150 significantly up-regulated genes, with 41 being CAZyme-encoding genes
375 (*p*-value $\leq$ 0.01) (**Fig. 3A**). The up-regulated CAZyme-encoding genes were diverse in
376 predicted activity, encompassing 10 putative carbohydrate-binding modules (CBMs),
377 eight pectinases, seven chitinases, four arabinanases, three glucanases, three
378 uncharacterized CAZymes, two mannanases, two cellulases, one xylanase, and one
379 amylase. Among the top 50 up-regulated genes (> 5.0-fold $\log_2$), the functional activities
380 observed were for gluconeogenesis, nutrient transport, and carbohydrate degradation
381 (**Table S5**). The CAZyme-encoding genes found within the top 50 up-regulated genes
382 included three chitinase-encoding genes (*cpin_2580, cpin_2186,* and *cpin_2184*), one
383 CBM-encoding gene with an encoded protein belonging to GH16 (*cpin_2187*), one
384 putative CBM-containing gene (*cpin_3792*), and one glucanase-encoding gene
385 (*cpin_5109*) (**Fig. 3D**). Notably, *cpin_2184, cpin_2186,* and *cpin_2187* belong to a fungal

386 cell wall utilization locus (FCWUL) and were recently renamed as *chiA, chiB,* and *glu16A,*
387 respectively (46).

388 Gene expression comparing growth on necromass during the exponential and
389 stationary phases (NecLo EXP vs NecLo STA) found up-regulation of 1,361 genes during
390 exponential growth, with 46 CAZyme-encoding genes (*p*-value ≤ 0.01) (**Fig. 3B**). Among
391 the 46 up regulated CAZyme-encoding genes included 10 chitinases, nine pectinases,
392 six putative CBMs (four of which contain GH2 domains), five glucanases, five
393 mannanases, five cellulases, four arabinanases, two galactanases, and one
394 uncharacterized CAZyme. Unsurprisingly, the top 50 up-regulated genes (> 3.4-fold $\log_2$)
395 identified genes encoding proteins important for cellular metabolism and growth. Gene
396 products included cobalamin synthesis, glycoside hydrolysis, cellular growth, and nutrient
397 transport (**Table S6**). The CAZyme-encoding genes identified within the top 50 up-
398 regulated genes included two β-glucanase (*cpin_5109* and *cpin_6736*) (**Fig. 3D**).
399 Differential expression analysis on glucose found that *cpin_6736* gene expression was
400 induced by growth rate and was part of a putative β-glucan utilization operon. Conversely,
401 *cpin_5109* was not in an operon and its expression was induced by both growth rate and
402 substrate presence, with stronger up-regulation in the presence of *H. bicolor* necromass.

403 The final differential expression analysis for *C. pinensis* compared stationary
404 phase on low melanin necromass to stationary phase on glucose (NecLo STA vs Glc
405 STA). Under these conditions, there were 1,092 up-regulated genes with 34 being
406 CAZyme-encoding genes (*p*-value ≤ 0.01) (**Fig. 3C**). In terms of CAZyme-encoding gene
407 expression, there were 34 up-regulated genes that included eight CBMs (one containing
408 a GH16 domain, one with a GH64 domain, one with a GH87 domain, and two with GH2

domains), six glucanases, six mannanases, five chitinases, three arabinanases, two pectinases, two cellulases, one xylanase, and one uncharacterized CAZyme. The top 50 up-regulated genes (> 6.0-fold log_2) encoded activities relative to bacterial respiration, TonB-dependent transport, and carbohydrate metabolism (**Table S7**). The CAZyme genes that were up-regulated more than 6.0-fold (log_2) were *cpin_2184* (*chiA*)*, cpin_2186* (*chiB*)*, cpin_2187* (*glu16A*)*,* and *cpin_1779* (**Fig. 3D**). As noted in the NecLo EXP vs Glc EXP comparison, *cpin_2184 – cpin_2187* belong to the recently characterized FCWUL.

C. japonicus has complex CAZyme-encoding gene expression during growth on necromass. Comparison of transcriptomic data collected during exponential growth on low melanin necromass compared to glucose was the most informative evaluation for *C. japonicus* gene expression. There were 1,077 up-regulated genes (p-value $\leq$ 0.01) with 100 being CAZyme-encoding genes which included 19 glucanases, 15 pectinases, nine cellulases, nine CBMs (two of which contain an AA10 domains), eight chitinases, seven amylases, six xylanases, six galactanases, eight arabinanases, four mannanases, four uncharacterized CAZymes, three acetylases, and two esterases (**Fig. 3E**). A complex gene expression response was not unsurprising for *C. japonicus* based on previous RNAseq studies (47), and 19 up-regulated glucanase-encoding genes would be expected based on glucans being the dominant polysaccharide found in *H. bicolor* cell walls. The top 50 up-regulated genes (> 5.3-fold log_2) encoded activities for ribosomal RNA, electron transport, and carbohydrate metabolism (**Table S11**). This list also included CAZyme-encoding genes *glu81A* (glucanase)*, cel5B* (cellulase)*, cbp26A* (CBM)*, chi18D* (chitinase)*, csn46F* (chitinosanase)*,* and *chi19A* (chitinase) (**Fig. 3H**). Notably, a *C.*

japonicus Δ*chi18D* mutant has previously been shown to be essential to *C. japonicus* α-chitin degradation, while Δ*chi19A* and Δ*csn46F* exhibited minor growth rate defects (48, 49).

C. japonicus growth on low melanin necromass during exponential growth compared to stationary phase had far fewer up-regulated CAZyme-encoding genes. In total, there were 548 up-regulated genes with 51 being CAZyme-encoding genes (*p*-value $\leq$ 0.01) (**Fig. 3F**). The 51 up-regulated CAZyme genes included eight glucanases, eight cellulases, five chitinases, five CBMs, four pectinases, three uncharacterized CAZymes, three esterases, three amylases, two xylanases, two arabinanases, one mannanase, and one galactanase. While fewer CAZyme-encoding genes were up-regulated, one-third of them were among the most up-regulated genes (top 50; $\geq$ 2.4-fold $\log_2$). The remaining genes expressed more than 2.4-fold ($\log_2$) encoded TonB-dependent transporters, cell wall biosynthesis proteins, and motility proteins (**Table S12**). The highly up-regulated CAZyme-encoding genes were *glu16B, glu81A, glu16A, cbp26A, cel6A, cel3C, cbp6B, cel5B, cbp2E, gly30A, glu5A, glu16F, pul13B, cbp2D, ce2C,* and *csn46F*, respectively (**Fig. 3H**). The high proportion of glucanase-encoding genes observed in this comparison provides ample targets for future physiological studies of *C. japonicus* CAZyme using gene deletion analyses during the degradation of fungal glucans.

Comparing the stationary phase on low melanin necromass with the stationary phase on glucose suggested some nutrient acquisition was still occurring in *C. japonicus* cells on low melanin necromass. There were 660 up regulated genes with 17 being CAZyme-encoding genes (*p*-value $\leq$ 0.01) (**Fig. 3G**). The CAZyme-encoding genes included six cellulases, two chitinases, two CBMs (both of which contain AA10 domains),

two pectinases, two uncharacterized CAZymes, one acetylase, and one trehalase. The top 50 up-regulated genes (> 3.1-fold log_2) encoded ribosomal RNA, nitrogen utilization proteins, and transposons (**Table S13**). Interestingly, this comparison lacked up-regulation of any CAZyme-encoding genes in the top 50 up-regulated genes. However, in the top 100 up-regulated genes (2.5-fold log_2) there were two CAZyme-encoding genes (*pel3B* and *pda4B*), which encode a pectate lyase and polysaccharide deacetylase, respectively (**Fig. 3H**).

***S. marcescens* exhibits a poor CAZyme-encoding gene expression response on necromass.** Corresponding with the poor growth of *S. marcescens* on *H. bicolor* necromass, this species elicited a sparse CAZyme-encoding gene expression response on that substrate. *S. marcescens* cells collected during exponential growth on low melanin necromass compared to glucose resulted in up-regulation of 1,130 genes with only nine encoding CAZymes (*p*-value $\leq$ 0.01) (**Fig. 3I**). Among the up-regulated CAZyme-encoding genes included three uncharacterized CAZymes, two CBMs, one chitinase, one glucanase, one cellulase, and one amylase. The top 50 up-regulated genes (> 5.2-fold log_2) encoded activities for transport, amino acid metabolism, and stress response (**Table S17**). While there were no CAZyme-encoding genes among the top 50 up-regulated genes, there were two included in the top 100, which were for a lytic polysaccharide monooxygenase (*L8N14_14090*) and a CBM (*L8N14_01950*) (**Fig. 3L**).

Growth of *S. marcescens* on low melanin necromass during exponential growth compared to stationary phase showed up-regulation of numerous genes involved in cell growth. There were 219 genes up-regulated with five CAZyme-encoding genes (*p*-value

≤ 0.01) (**Fig. 3J**). Among the up-regulated CAZyme-encoding gene included two chitinases, two uncharacterized CAZymes, and one CBM. The top 50 up-regulated genes (> 1.7-fold $\log_2$) encoded activities such as carbohydrate metabolism, transcriptional regulators, and transporters (**Table S18**). Unlike the exponential growth phase comparisons, here, the top 50 up-regulated genes included the CAZyme-encoding genes *L8N14_14080, L8N14_01950, L8N14_14090,* and *L8N14_01905.* These are predicted to encode a chitinase, CBM, lytic polysaccharide monooxygenase, and another chitinase, respectively *(***Fig. 3L**).

Our final comparison comprised of *S. marcescens* during stationary phase on low melanin necromass compared to glucose. Here we observed up-regulation of 730 genes with seven being CAZyme-encoding genes (*p*-value ≤ 0.01) (**Fig. 3K**). The top 50 up-regulated genes (> 2.7-fold $\log_2$) encoded activities for nutrient transport, ribosomal RNA, and cell wall repair (**Table S19**). However, far fewer CAZyme-encoding genes were up-regulated in these conditions. Only two chitinases, two glucanases, two cellulases, and one amylase were identified, however, none were among the top 50 or even top 100 up-regulated genes. In fact, the chitinase-encoding gene (*L8N14_22810*) was the most up-regulated CAZyme encoding gene with a 1.7-fold expression change ($\log_2$).

Gene expression of nitrogen utilization-encoding genes was highly variable across species grown on necromass. Previous reports have indicated that the high melanin type of *H. bicolor* has significantly less nitrogen than the low melanin type (23). Despite supplementation of ammonia in the growth medium, we still observed differences in the gene expression response of *S. marcescens* and *C. pinensis* under conditions which

compared exponential growth on necromass versus glucose as well as stationary phase on necromass versus glucose (**Table S23**). Similar to the CAZyme-encoding gene expression response, expression comparisons of nitrogen utilization-encoding genes were highly similar between the high and low necromass substrates (**Table S6, S9, S12, S15, S18, S21**). Interestingly, however, all three species up-regulated a different set of nitrogen utilization-encoding genes during exponential growth on glucose (Glc EXP vs Glc STA) than on necromass (Nec EXP vs Glc EXP) (**Table S23**). Considering this, we hypothesize that the up-regulated nitrogen utilization-encoding genes are likely important for nitrogen acquisition from necromass and are not solely reflective of growth rate-dependent gene expression.

During exponential growth (NecLo EXP vs Glc EXP), *C. pinensis* up-regulated four nitrogen utilization genes (*cpin_2006, cpin_3374, cpin_1695,* and *cpin_0230*) on low melanin necromass compared to glucose (**Table S23; Table S5**). Comparatively, only *cpin_1695* was also up-regulated during exponential growth on high melanin necromass compared to glucose (**Table S8**). During stationary phase, *C. pinensis* on low melanin necromass elicited up-regulation of *cpin_4284*, *cpin_0230*, *cpin_1695*, and *cpin_5012* (**Table S23 and Table S7**). The stationary phase *C. pinensis* response on high melanin necromass only up-regulated *cpin_0230* (**Table S10**). Interestingly, *C. pinensis* did not up-regulate any of the same nitrogen utilization-encoding genes on low melanin necromass compared to those during exponential growth on glucose. Instead, *C. pinensis* up-regulated genes that encoded nitroreductases, nitropropane dioxygenases, and nitrogen-fixing proteins when grown on necromass compared to glucose.

S. marcescens up-regulated the most nitrogen-utilization encoding genes on necromass compared to glucose. During exponential growth on low melanin necromass (NecLo EXP vs Glc EXP), nine *S. marcescens* nitrogen utilization-encoding genes were up-regulated, which included *L8N14_11925*, *L8N14_06450*, *L8N14_10750*, *L8N14_04185*, *L8N14_21470*, *L8N14_16415*, *L8N14_18380*, *L8N14_13885*, *L8N14_10745*, *L8N14_18910*, and *L8N14_15185* (**Table S23 and Table S17**). On high melanin necromass (NecHi EXP vs Glc EXP), the up-regulated genes during exponential growth were *L8N14_11925, L8N14_06450,* and *L8N14_21470* (**Table S20**). During stationary phase on low melanin necromass, *S. marcescens* up-regulated *L8N14_21965*, *L8N14_05810*, *L8N14_24000*, *L8N14_23630*, *L8N14_12535*, *L8N14_03515*, and *L8N14_18910* (**Table S23 and S19**). During stationary phase on high melanin necromass, the up-regulated genes were *L8N14_04185, L8N14_21965*, *L8N14_23630*, *L8N14_12535*, and *L8N14_05810* (**Table S22**). Overall, the only nitrogen utilization-encoding genes that were up-regulated in both the Glc EXP vs Glc STA and Nec STA vs Glc STA comparisons were four genes which encoded a nitrite reductase, carbon-nitrogen hydrolase, nitrogen regulation protein, and glutamine synthetase (**Table S23**).

During exponential growth on necromass compared to glucose (Nec EXP vs Glc EXP)*, C. japonicus* up-regulated seven nitrogen utilization genes (*cja_2161, ald, cja_3392, ntrC, norB, cja_3390, nirB,* and *nirD*) (**Table S23; Table S11; Table S14**). During stationary phase on low melanin necromass compared to glucose (Nec STA vs Glc STA), *C. japonicus* up-regulated nine nitrogen utilization genes that included *cja_3392*, *glnA*, *ntrC*, *nirB*, *nirD*, *cja_3390*, *cja_3536*, *gltD*, and *gltB* (**Table S23 and S13**). Comparatively, stationary phase on high melanin necromass up-regulated the same set

546 of genes, although *cja_3536* was absent and *cja_1973* was present, which encodes the
547 α subunit of glutamate synthase (**Table S16**). Among the up-regulated nitrogen utilization-
548 encoding genes on necromass*,* the only genes that were also up-regulated on glucose
549 (Glc EXP vs Glc STA) were expressed during stationary phase on necromass*.* These
550 encoded a glutamine synthetase (*glnA*) and glutamate synthase (*gltD*).
551
552 **CARBON AND NITROGEN UTILIZATION ANALYSES**
553 To better characterize the metabolic potential of *C. pinensis, C. japonicus,* and *S.*
554 *marcescens*, we assessed the metabolic phenotypes of the three species on a broad
555 range of carbon and nitrogen sources (**Fig. 4 and Table S24-26**). These assays yielded
556 multiple intriguing results, for example the poor metabolic activity of *C. pinensis* on
557 glucose. As demonstrated in **Fig. S1**, this strain can grow well on glucose as a sole carbon
558 source. These differences may be a consequence of the BioLog system, which assesses
559 bacterial metabolic respiration and not growth. Moreover, the BioLog system has a
560 universal bacterial assay design, therefore it is possible that the tested substrates could
561 be better optimized for utilization studies. Despite these limitations, the BioLog
562 experiments were able to assay a broad range of substrates and further inform our models
563 for carbon and nitrogen metabolism of the three bacterial species they pertain to
564 necromass utilization.
565 The poor metabolic activity of *C. pinensis* on α-mannan was a surprising
566 phenotype considering the strain has 10 predicted α-mannanases (45). However, D-
567 mannose was the only relevant monosaccharide that elicited high metabolic activity by *C.*
568 *pinensis* (**Fig. 4A, D, & G**). The strain also exhibited high metabolic activity on

569 glucosamine and *N*-acetylglucosamine compared to the mannose- and galactose-based
570 amino sugars. Additionally, *C. pinensis* could utilize L-amino acids as sole nitrogen
571 sources but had poor metabolic activity when provided with the same substrates as sole
572 carbon sources, with one exception being L-aspartic acid. Overall, *C. pinensis* was most
573 metabolically active on nitrite, nitrate, and urea.

574 In addition to the poor metabolic activity of *C. japonicus* on α-mannan, the strain
575 also had poor activity on D-mannose, as has been previously recorded (47, 50).
576 Alternatively, *C. japonicus* exhibited high metabolic activity on D-galactose and D-
577 glucose. This was also true on the glucose-based amino sugars glucosamine and *N*-
578 acetylglucosamine when utilized as carbon sources (**Fig. 4B, E, & H**). A lack of metabolic
579 activity by *C. japonicus* was observed on L-amino acids as either carbon or nitrogen
580 sources. In fact, the only nitrogen sources that *C. japonicus* exhibited high metabolic
581 activity on were nitrite, nitrate, and urea.

582 *S. marcescens* had the broadest metabolic range of the three strains on carbon
583 and nitrogen sources assayed. *S. marcescens* had very high activity on D-glucose, D-
584 galactose, D-mannose, and the amino sugars, with the sole exception being *N*-acetyl
585 mannosamine (**Fig. 4C, F, & I**). The amino sugars also provided *S. marcescens* with a
586 small amount of activity when provided as a sole nitrogen source. When grown on L-
587 amino acids as either carbon or nitrogen sources, *S. marcescens* was highly metabolically
588 active. Activity was highest on the L-amino acids when the strain utilized them for nitrogen
589 compared to carbon. Finally, testing *S. marcescens* metabolic activity on canonical
590 nitrogen sources (nitrite, nitrate, ammonia, urea) indicated all four could be utilized, with
591 ammonia and urea eliciting the highest activity.

DISCUSSION

The decomposition of fungal necromass has been shown to significantly contribute to the both carbon and nitrogen cycling in forest soils (51). Therefore, understanding the mechanisms of its decay and the saccharifying properties of its decomposers is important to understand the dynamics of soil nutrients, as recently reviewed (24). The use of *Hyaloscypha bicolor* as a model necromass benefits this area of research through its potential to exist in chemically distinct but genetically equivalent phenotypes. Previous chemical analysis of the *H. bicolor* cell wall has shown that the low melanin type contains twice the carbohydrates as the high melanin type, making carbohydrates roughly 40% of the low melanin *H. bicolor* cell wall (23). Interestingly, despite the difference in polysaccharide proportions between the two types of *H. bicolor,* the CAZyme-encoding gene expression responses of all three bacteria were almost identical on both necromass types (**Fig. 3 and S2**). While the exact concentrations of each polysaccharide in the *H. bicolor* cell wall are still unknown, other fungal species belonging to the phylum *Ascomycota* (e.*g. Yarrowia lipolytica, Aspergillus fumigatus,* and *Candida albicans*) had glycan content ranging between 45-60% glucans and 16-20% chitin (52–54). Our pyGCMS analysis of *H. bicolor* revealed a somewhat lower glycan content (~29% carbohydrate) and chitin content (~13% of N-containing compounds, which includes proteins and amino sugars like chitin) (**Table S27**). Future work parsing amino sugars from amino acids and determining the glucan content of *H. bicolor* cell walls with different levels of melanization will facilitate more accurate comparisons to other fungi.

The signals that elicit the observed CAZyme-encoding gene expression responses are clearly similar, suggesting that melanization does not impact bacterial carbon

utilization gene expression, at least under the assay conditions used. However, these necromass variants are particularly interesting when considering the notable differences in gene expression of the nitrogen utilization-encoding genes of *C. pinensis* and *S. marcescens* on high versus low melanin necromass (**Table S23**). Collectively, these results complement *H. bicolor* decomposition studies wherein nitrogen appears to be a substantial factor to its degradation (18, 21, 22, 55).

Chitinophaga pinensis is an early-stage necromass degrader with metabolic potential to persist into later stages. *C. pinensis* exhibited the quickest transition to exponential growth on both types of necromass (**Fig. 1**). This is likely due to its growth-rate dependent CAZyme-encoding gene expression response since neither of the other strains elicited a response quite as broad as *C. pinensis* during exponential growth on glucose compared to stationary phase. The up-regulated CAZyme-encoding genes in this growth comparison overwhelmingly encoded mannanase gene products, followed by cellulases, chitinases, glucanases, and arabinanases (**Fig. 2**). Notably, up-regulation of chitinase-, glucanase-, and mannanase-encoding genes upon entrance into exponential growth logically increases the adaptability of *C. pinensis* to grow on fungal necromass. This observed specialty of *C. pinensis* to quickly adapt to its substrate was partly conveyed *in situ.* A study on bacterial genera presence during various phases of *H. bicolor* decomposition showed *Chitinophaga* was among the dominant genera during the early- and mid-stages of decay (21). Interestingly, however, *Chitinophaga* has also been identified as the dominating genus during late-stage degradation of necromass associated with plant hosts (21), which could be either due to flexible metabolic capacity

638 or potentially the decomposition of newly senescent microbes that were themselves a
639 part of the early necromass decomposition community.

640 Despite the broad CAZyme-encoding gene expression response of *C. pinensis*
641 during exponential growth, this species had a more specific response when grown on
642 necromass (**Fig. 3A-D**). In the NecLo EXP vs Glc EXP comparison, the chitinase-,
643 glucanase- and CBM-encoding genes were among the most up-regulated. However, one
644 of the more revealing comparisons was in NecLo EXP vs NecLo STA and NecLo STA vs
645 Glc STA. There, the NecLo EXP vs NecLo STA comparison overwhelmingly encoded β-
646 glucanases. This varied from the NecLo STA vs Glc STA comparison which up-regulated
647 more chitinase-encoding genes. This adjustment to the expression response could be
648 reflective of polysaccharide presence, wherein the outer β-glucan layer of *H. bicolor* has
649 been deconstructed enough to reveal the chitinous inner layer of the substrate.
650 Alternatively, increases in chitinase gene expression during stationary phase could
651 instead be an attempt at nitrogen acquisition since the strain can utilize *N*-
652 acetylglucosamine and glucosamine as nitrogen sources (**Fig. 4**). Moreover, the
653 combined broad expression of CAZyme-encoding genes during exponential growth
654 paired with substrate-specific induced expression of β-glucanases contributes to our
655 hypothesis that *C. pinensis* would prevail as the early-stage degrader among the three
656 species (**Fig. 5**). Two polysaccharide utilization loci (PUL) appeared to be most
657 prevalently expressed. These PULs encompass *cpin_6730* – *cpin_6742* and *cpin_2184*
658 – *cpin_2192.* The former was up-regulated during exponential growth and encodes for an
659 endo-β-1,3-glucanase, endo-β-1,6-glucanase, and an exo-β-glucosidase (56). The latter
660 PUL belongs to a recently identified and characterized fungal cell wall utilization locus

(FCWUL) (46). The poor metabolic activity of *C. pinensis* when grown on α-mannan alone was a surprising result. Analysis of the predicted PULs in *C. pinensis* indicate nine of its α-mannanase-encoding genes lie within PULs, however none of these PULs possess more than one α-mannanase-encoding gene or any other fungal cell wall-degrading CAZyme (57). Interestingly, *C. pinensis* has been shown to grow on plant β-mannans such as konjac glucomannan and carob galactomannan (45, 58), but there have been no growth studies of the bacterium on chitin.

C. pinensis exhibited changes in gene expression of nitrogen utilization-encoding genes on high versus low melanin necromass (**Table S23**). These differences were observed between the two necromass types and between the two growth phases. Exponential growth on low melanin versus high melanin necromass (Nec EXP vs Glc EXP) resulted in a higher number of up-regulated genes important to nitrogen acquisition from amino acids (*cpin_2006* and *cpin_3374*). This differed from the up-regulated nitrogen utilization-encoding genes during stationary phase on low versus high melanin necromass, which up-regulated two nitroreductase-encoding genes (*cpin_4284* and *cpin_5012*). While little is known about nitrogen metabolism in *C. pinensis,* these results may indicate that a higher protein presence may exist in the cell wall of low melanin necromass from which *C. pinensis* can derive its nitrogen. An alternative hypothesis is that fungal proteins are better protected from degradation in high melanin cell walls, so the observed increase in gene expression under the low melanin conditions is because fungal proteins are more accessible.

683 ***C. japonicus has exceptional efficiency during polysaccharide degradation as a***
684 ***mid-stage degrader of necromass.*** Growth on fungal cell wall degradation products
685 showed *C. japonicus* is highly active on the canonical polysaccharide constituents
686 (glucose, glucosamine, and *N*-acetylglucosamine), with little metabolic activity on other
687 amino sugars (**Fig. 4**). Notably, *C. japonicus* had the fastest growth rates on both
688 necromass types despite having a longer lag phase than *C. pinensis* (**Table S2**). Since
689 *C. japonicus* has all the necessary CAZymes to completely degrade the fungal cell wall
690 and has a faster growth rate on necromass, we suggest this species to be a strong
691 candidate for a versatile mid-stage degrader of necromass (**Fig. 5**).

692 *C. japonicus* has an extensive history of transcriptomic and mutational analyses
693 on various polysaccharides during different growth phases (42, 47, 49, 59). Notably, the
694 CAZyme-encoding gene expression response of *C. japonicus* on low melanin *H. bicolor*
695 necromass has thus far been the only substrate to elicit such strong up-regulation of non-
696 cellulase, β-glucanase-encoding genes. The predicted glucanases largely belong to
697 GH16 and GH81 which hydrolyze diverse sugar linkages and β-1,6-glucans, respectively
698 (25, 60). Within the highly up-regulated CAZyme-encoding genes during exponential
699 growth on necromass compared to glucose, the only strongly up-regulated β-glucanase-
700 encoding gene was *glu81A.* However, the response of *C. japonicus* cells grown on *H.*
701 *bicolor* during exponential growth compared to stationary phase strongly up-regulated
702 *glu81A, glu16A, glu16B,* and *glu16F* (**Fig. 3F**). Similarly, the major *C. japonicus*
703 chitinolytic machinery has been characterized via a combination of mutational,
704 biochemical, and secretome studies (48, 49, 61). During exponential growth on
705 necromass compared to glucose, *chi18D, csn46F,* and *chi19A* were strongly up-regulated

(**Fig. 3E**). Previous physiological studies identified Chi18D as an essential chitinase to the degradation of α-chitin and crab shells, followed by Chi18A-C (48). However, mutational analyses of *chi19A* and *csn46F* grown on α-chitin and crab shell resulted in subtle changes in growth compared to wild-type (49). Finally, the *C. japonicus* chitinolytic suite also contains LPMO10A, which is known to be physiologically important for *C. japonicus* growth on α-chitin and present in high quantities in the secretome of α-chitin grown cells (61, 62). Interestingly, expression of the corresponding gene was only up-regulated in the NecLo EXP vs Glc EXP and NecLo STA vs Glc STA comparisons, and not at all up-regulated in NecLo EXP vs NecLo STA. Instead, the gene encoding the cellulose-binding LPMO (*lpmo10B*) was more frequently up-regulated (**Table S11-S16**).

C. japonicus was the only species that did not elicit distinguishing differences in the expression of nitrogen utilization-encoding genes based on necromass melanization (**Table S23**). Assessment of its metabolic activity on various nitrogen sources indicate *C. japonicus* has extremely poor activity on peptides and amino acids, which verifies previous growth studies (32). Rather than necromass-induced changes to the expression of nitrogen utilization-encoding genes, *C. japonicus* exhibited minor differences between exponential growth and stationary phase on *H. bicolor*. Stationary phase on either necromass type elicited up regulation of *glnA, gltD,* and *gltB*, which encode a glutamine synthetase and two glutamate synthases, respectively. Notably, up-regulation of a glutamine synthetase-encoding gene during stationary phase is a well-documented occurrence in bacteria and does not appear to be indicative of a unique response to fungal necromass (63–66).

S. marcescens could fill the ecological role of a late-stage necromass degrader. *S. marcescens* exhibited the greatest metabolic activity on the fungal cell wall derivatives and amino acids, however its growth on necromass was poor (**Fig. 1 and 4**). The lack of any CAZymes belonging to the families GH5, GH16, GH17, and GH30 is likely the cause for the poor growth since these are typically active on β-1,3- and β-1,6-glucans (25, 28). A previous growth assessment of *S. marcescens* on *Aspergillus nidulans* showed the strain had similarly poor growth dynamics compared to α-chitin and glucose (44). Since the structure of fungal cell walls generally have β-glucans as the outer most layer, the observed poor growth could be due to the limited access to chitin (13). Therefore, we suspect that *S. marcescens* would most likely be a late-stage degrader of necromass after the other microbial decomposers have removed the impeding β-glucans (**Fig. 5**).

CAZyme-encoding gene expression of *S. marcescens* during exponential growth on glucose compared to stationary phase was much more modest than that observed for *C. pinensis* (**Fig. 2**). Only nine CAZyme-encoding genes were up-regulated and mostly included those relevant to chitin and glucan hydrolysis. Considering that *S. marcescens* does not have any CAZymes belonging to the fungal glucan-degrading GH families, the three up-regulated glucanase-encoding genes (which encode 6-phospho-β-glucosidases) are unlikely to be important to fungal necromass decomposition. However, there were up-regulated GH18 class chitinase-encoding genes as well as one *N*-acetyl-β-hexosaminidase encoding gene also up-regulated. Despite a limited and overall growth rate-dependent CAZyme-encoding gene expression response, *S. marcescens* clearly prioritizes the utilization of chitin by rapidly expressing nearly all its chitinase-encoding genes based solely on growth rate. This preparation for chitin exposure suggests that *S.*

752 *marcescens* abundance might increase during late-stage decomposition when chitin is
753 potentially the primary remaining nitrogen source remaining. *S. marcescens* has a well-
754 studied chitinase system which includes three chitinases belonging to GH18 and an
755 LPMO from AA10 (67–69), and as possessing a model chitinolytic system (70), *S.*
756 *marcescens* likely out-competes other microbes during late-stage necromass decay.
757 Similar to *C. pinensis, S. marcescens* had altered expression of nitrogen utilization-
758 encoding genes on the high versus low melanin necromass. During exponential growth
759 on the low melanin necromass*, S. marcescens* up-regulated almost three times the
760 nitrogen utilization-encoding genes compared to exponential growth on high melanin
761 necromass (**Table S23**). Since *S. marcescens* growth on necromass was sparse,
762 expression of several glutamine synthetases may have increased as part of a starvation
763 response (66, 71).
764
765 ***Concluding remarks.*** To gain a predictive capacity of necrobiome composition and
766 dynamics, research requires an integrated approach, starting with community
767 characterization and moving towards mechanisms of substrate degradation, followed by
768 experimental studies in community settings. In this study, we have transcriptomically
769 characterized three bacterial species during necromass decomposition and provided a
770 series of hypotheses concerning their contribution to necromass decay *in vivo*. Our results
771 indicate that melanin content of *H. bicolor* necromass elicits the same CAZyme-encoding
772 gene expression responses in *C. japonicus*, *C. pinensis*, and *S. marcescens*. Considering
773 the growth capabilities and gene expression responses collectively, we present a model

774 of different niches for each species during decomposition from which more detailed
775 genetic and biochemical studies of microbial necromass degraders can build.
776

ACKNOWLEDGEMENTS

This work was supported by the National Science Foundation under Award Number DEB2038304. The authors thank Dr. Jennifer Pett-Ridge at Lawrence Livermore National Laboratory, Dr. Jonathan Schilling from University of Minnesota, Dr. François Maillard at Lund University, Sweden for helpful discussions over the course of this work, and Kathryn Schreiner and Julia Agnich at the University of Minnesota - Duluth for their contributions to the pyGCMS work. We also acknowledge the Joint Genome Initiative “Defining the Populus Microbiome” Project, from which the *H. bicolor* isolate used for necromass was derived.

AUTHOR CONTRIBUTIONS

JKN performed the RNAseq analysis and led the manuscript writing at UMBC.

PGK supervised the work at UMN and contributed to writing the manuscript.

JGG designed the study, supervised the work at UMBC, and contributed to writing the manuscript. All authors read and approved the final submitted version of the manuscript.

COMPLIANCE WITH ETHICAL STANDARDS

This article does not contain any experiments using human participants or animals. The authors also declare that they have no conflicts of interest.

DISCLAIMER

REFERENCES

1. Fernandez CW, See CR, Kennedy PG. 2020. Decelerated carbon cycling by ectomycorrhizal fungi is controlled by substrate quality and community composition. New Phytol 226:569–582.
2. Saifuddin M, Bhatnagar JM, Phillips RP, Finzi AC. 2021. Ectomycorrhizal fungi are associated with reduced nitrogen cycling rates in temperate forest soils without corresponding trends in bacterial functional groups. Oecologia 196:863–875.
3. Lindahl BD, Kyaschenko J, Varenius K, Clemmensen KE, Dahlberg A, Karltun E, Stendahl J. 2021. A group of ectomycorrhizal fungi restricts organic matter accumulation in boreal forest. Ecol Lett 24:1341–1351.
4. Wang F, Zhang L, Zhou J, Rengel Z, George TS, Feng G. 2022. Exploring the secrets of hyphosphere of arbuscular mycorrhizal fungi: processes and ecological functions. Plant Soil 481:1–22.
5. Cairney JWG. 2011. Ectomycorrhizal fungi: The symbiotic route to the root for phosphorus in forest soils. Plant Soil 344:51–71.
6. Jeffries P, Gianinazzi S, Perotto S, Turnau K, Barea JM. 2003. The contribution of arbuscular mycorrhizal fungi in sustainable maintenance of plant health and soil fertility. Biol Fertil Soils 37:1–16.
7. Bukovská P, Rozmoš M, Kotianová M, Gančarčíková K, Dudáš M, Hršelová H, Jansa J. 2021. Arbuscular Mycorrhiza Mediates Efficient Recycling From Soil to Plants of Nitrogen Bound in Chitin. Front Microbiol 12:1–16.
8. Liu Y, Li X, Kou Y. 2020. Ectomycorrhizal fungi: Participation in nutrient turnover

and community assembly pattern in forest ecosystems. Forests 11:1–16.

9. Clemmensen KE, Bahr A, Ovaskainen O, Dahlberg A, Ekblad A, Wallander H, Stenlid J, Finlay RD, Wardle DA, Lindahl BD. 2013. Roots and Associated Fungi Drive Long-Term Carbon Sequestration in Boreal Forest. Sci Reports 339:1615–1618.

10. Cantoran A, Maillard F, Baldrian P, Kennedy PG. 2023. Defining a core microbial necrobiome associated with decomposing fungal necromass. FEMS Microbiol Ecol 99:1–11.

11. Zeglin LH, Myrold DD. 2013. Fate of Decomposed Fungal Cell Wall Material in Organic Horizons of Old-Growth Douglas-fir Forest Soils. Soil Sci Soc Am J 77:489–500.

12. Feofilova EP. 2010. The Fungal Cell Wall: Modern Concepts of Its Composition. Microbiology 79:711–720.

13. Gow NAR, Latge J-P, Munro CA. 2017. The Fungal Cell Wall: Structure, Biosynthesis, and Function. Microbiol Spectr 5.

14. van der Wal A, Bloem J, Mulder C, de Boer W. 2009. Relative abundance and activity of melanized hyphae in different soil ecosystems. Soil Biol Biochem 41:417–419.

15. Eisenman HC, Casadevall A. 2012. Synthesis and assembly of fungal melanin. Appl Microbiol Biotechnol 93:931–940.

16. Pihet M, Vandeputte P, Tronchin G, Renier G, Saulnier P, Georgeault S, Mallet R, Chabasse D, Symoens F, Bouchara JP. 2009. Melanin is an essential component for the integrity of the cell wall of Aspergillus fumigatus conidia. BMC Microbiol

9:1–11.

17. Nosanchuk JD, Stark RE, Casadevall A. 2015. Fungal melanin: What do we know about structure? Front Microbiol 6:1–7.

18. Fernandez CW, Koide RT. 2014. Initial melanin and nitrogen concentrations control the decomposition of ectomycorrhizal fungal litter. Soil Biol Biochem 77:150–157.

19. Xu C, Li J, Yang L, Shi F, Yang L, Ye M. 2017. Antibacterial activity and a membrane damage mechanism of Lachnum YM30 melanin against Vibrio parahaemolyticus and Staphylococcus aureus. Food Control 73:1445–1451.

20. Fehrer J, Réblová M, Bambasová V, Vohník M. 2019. The root-symbiotic Rhizoscyphus ericae aggregate and Hyaloscypha (Leotiomycetes) are congeneric: Phylogenetic and experimental evidence. Stud Mycol 92:195–225.

21. Fernandez CW, Kennedy PG. 2018. Melanization of mycorrhizal fungal necromass structures microbial decomposer communities. J Ecol 106:468–479.

22. Fernandez CW, Heckman K, Kolka R, Kennedy PG. 2019. Melanin mitigates the accelerated decay of mycorrhizal necromass with peatland warming. Ecol Lett 1–8.

23. Ryan ME, Schreiner KM, Swenson JT, Gagne J, Kennedy PG. 2020. Rapid changes in the chemical composition of degrading ectomycorrhizal fungal necromass. Fungal Ecol 45:100922.

24. Kennedy PG, Maillard F. 2023. Knowns and unknowns of the soil fungal necrobiome. Trends Microbiol 31:173–180.

25. Starke R, Morais D, Vetrovsky T, Mondéjar RL, Baldrian P, Brabcová V. 2020.

878 Feeding on fungi: genomic and proteomic analysis of the enzymatic machinery of
879 bacteria decomposing fungal biomass. Environ Microbiol 22:4604–4619.
880 26. Deboy RT, Mongodin EF, Fouts DE, Tailford LE, Khouri H, Emerson JB,
881 Mohamoud Y, Watkins K, Henrissat B, Gilbert HJ, Nelson KE. 2008. Insights into
882 Plant Cell Wall Degradation from the Genome Sequence of the Soil Bacterium
883 Cellvibrio japonicus. J Bacteriol 190:5455–5463.
884 27. Watanabe T, Kimura K, Sumiya T, Nikaidou N, Suzuki K, Suzuki M, Taiyoji M,
885 Ferrer S, Regue M. 1997. Genetic analysis of the chitinase system of Serratia
886 marcescens 2170. J Bacteriol 179:7111–7117.
887 28. Lu Z, Rämgård C, Ergenlioğlu İ, Sandin L, Hammar H, Andersson H, King K,
888 Inman AR, Hao M, Bulone V, McKee LS. 2023. Multiple enzymatic approaches to
889 hydrolysis of fungal β-glucans by the soil bacterium Chitinophaga pinensis. FEBS
890 J 290:2909–2922.
891 29. Rokem JS, Klein D, Toder H, Zomer E. 1986. Degradation of fungal cell walls
892 taking into consideration the polysaccharide composition. Enzyme Microb Technol
893 8:588–592.
894 30. Sivan A, Chet I. 1989. Degradation of Fungal Cell Walls by Lytic Enzymes of
895 Trichoderma harzianum. Microbiology 135:675–682.
896 31. Grifoll-Romero L, Pascual S, Aragunde H, Biarnés X, Planas A. 2018. Chitin
897 deacetylases: Structures, specificities, and biotech applications. Polymers (Basel)
898 10:1–29.
899 32. Gardner JG, Keating DH. 2012. Genetic and functional genomic approaches for
900 the study of plant cell wall degradation in Cellvibrio japonicus. Methods Enzymol

510:331–347.

33. Picardi E. 2021. RNA Bioinformatics Methods in Molecular Biology.

34. Gruening BA. 2014. Concatenate datasets tail-to-head (cat). https://github.com/bgruening/galaxytools.

35. Andrews S. 2010. Fastqc A Quality Control Tool For High Throughput Sequence Data. http://www.bioinformatics.babraham.ac.uk/projects/fastqc.

36. Kim D, Langmead B, Salzberg SL. 2015. HISAT : a fast spliced aligner with low memory requirements. Nat Methods 12:357–362.

37. Anders S, Pyl PT, Huber W. 2015. Genome analysis HTSeq — a Python framework to work with high-throughput sequencing data. Bioinformatics 31:166–169.

38. Love MI, Huber W, Anders S. 2014. Moderated estimation of fold change and dispersion for RNA-seq data with DESeq2. Genome Biol 15:1–21.

39. Scaria J, Chen JW, Useh N, He H, McDonough SP, Mao C, Sobral B, Chang YF. 2014. Comparative nutritional and chemical phenome of Clostridium difficile isolates determined using phenotype microarrays. Int J Infect Dis 27:20–25.

40. Khatri B, Fielder M, Jones G, Newell W, Abu-Oun M, Wheeler PR. 2013. High Throughput Phenotypic Analysis of Mycobacterium tuberculosis and Mycobacterium bovis Strains' Metabolism Using Biolog Phenotype Microarrays. PLoS One 8.

41. Gardner JG, Crouch L, Labourel A, Forsberg Z, Bukhman Y V, Vaaje-kolstad G, Gilbert HJ, Keating DH. 2014. Systems biology defines the biological significance of redox-active proteins during cellulose degradation in an aerobic bacterium

924 94:1121–1133.
925 42. Nelson CE, Rogowski A, Morland C, Wilhide JA, Gilbert HJ, Gardner JG. 2017.
926 Systems analysis in Cellvibrio japonicus resolves predicted redundancy of b -
927 glucosidases and determines essential physiological functions. Mol Microbiol
928 104:294–305.
929 43. Larsbrink J, Tuveng TR, Pope PB, Bulone V, Eijsink VGH, Brumer H, McKee LS.
930 2017. Proteomic data on enzyme secretion and activity in the bacterium
931 Chitinophaga pinensis. Data Br 11:484–490.
932 44. Novak JK, Gardner JG. 2022. Draft Genome Sequence of a Serratia marcescens
933 Strain (PIC3611) Proficient at Recalcitrant Polysaccharide Utilization. Microb
934 Resour Announc 11:12–14.
935 45. Larsbrink J, Tuveng TR, Pope PB, Bulone V, Eijsink VGH, Brumer H, Mckee LS.
936 2017. Proteomic insights into mannan degradation and protein secretion by the
937 forest fl oor bacterium Chitinophaga pinensis. J Proteomics 156:63–74.
938 46. Lu Z, Kvammen A, Li H, Hao M, Inman AR, Bulone V, Mckee LS. 2023. A
939 polysaccharide utilization locus from Chitinophaga pinensis simultaneously
940 targets chitin and β-glucans found in fungal cell walls. mSphere 8.
941 47. Novak JK, Gardner JG. 2023. Galactomannan utilization by Cellvibrio japonicus
942 relies on a single essential α-galactosidase encoded by the aga27A gene. Mol
943 Microbiol 119:312–325.
944 48. Monge EC, Tuveng TR, Vaaje-Kolstad G, Eijsink VGH, Gardner JG. 2018.
945 Systems analysis of the glycoside hydrolase family 18 enzymes from Cellvibrio
946 japonicus characterizes essential chitin degradation functions. J Biol Chem

293:3849–3859.

49. Monge EC, Gardner JG. 2021. Efficient chito-oligosaccharide utilization requires two TonB-dependent transporters and one hexosaminidase in Cellvibrio japonicus. Mol Biol 116:366–380.

50. Humphry DR, Black GW, Cummings SP. 2003. Reclassification of “Pseudomonas fluorescens subsp. cellulosa” NCIMB 10462 (Ueda et al. 1952) as Cellvibrio japonicus sp. nov. and revival of Cellvibrio vulgaris sp. nov., nom. rev. and Cellvibrio fulvus sp. nov., nom. rev. Int J Syst Evol Microbiol 53:393–400.

51. Godbold DL, Hoosbeek MR, Lukac M, Cotrufo MF, Janssens IA, Ceulemans R, Polle A, Velthorst EJ, Scarascia-Mugnozza G, Angelis P De, Miglietta F, Peressotti A. 2006. Mycorrhizal hyphal turnover as a dominant process for carbon input into soil organic matter. Plant Soil 281:15–24.

52. Vega R, Domínguez A. 1986. Cell wall composition of the yeast and mycelial forms of Yarrowia lipolytica. Arch Microbiol 144:124–130.

53. Kang X, Kirui A, Muszyński A, Widanage MCD, Chen A, Azadi P, Wang P, Mentink-Vigier F, Wang T. 2018. Molecular architecture of fungal cell walls revealed by solid-state NMR. Nat Commun 9:1–12.

54. Garcia-Rubio R, de Oliveira HC, Rivera J, Trevijano-Contador N. 2020. The Fungal Cell Wall: Candida, Cryptococcus, and Aspergillus Species. Front Microbiol 10:1–13.

55. Maillard F, Michaud TJ, See CR, DeLancey LC, Blazewicz SJ, Kimbrel JA, Pett-Ridge J, Kennedy PG. 2023. Melanization slows the rapid movement of fungal necromass carbon and nitrogen into both bacterial and fungal decomposer

970 communities and soils. mSystems 8.
971 56. Mckee LS, Ruthes AC, Vilaplana F, Brumer H. 2023. Focused Metabolism of B-
972 Glucans by the Soil Bacteroidetes Species Chitinophaga pinensis. Appl Environ
973 Microbiol 85:e02231-18.
974 57. Terrapon N, Lombard V, Drula É, Lapébie P, Al-Masaudi S, Gilbert HJ, Henrissat
975 B. 2018. PULDB: The expanded database of Polysaccharide Utilization Loci.
976 Nucleic Acids Res 46:D677–D683.
977 58. McKee LS, Brumer H. 2015. Growth of Chitinophaga pinensis on plant cell wall
978 glycans and characterisation of a glycoside hydrolase family 27 β-L-
979 arabinopyranosidase implicated in arabinogalactan utilisation. PLoS One 10:1–22.
980 59. Blake AD, Beri NR, Guttman HS, Cheng R, Gardner JG. 2018. The complex
981 physiology of Cellvibrio japonicus xylan degradation relies on a single cytoplasmic
982 β-xylosidase for xylo-oligosaccharide utilization. Mol Microbiol 107:610–622.
983 60. Viborg AH, Terrapon N, Lombard V, Michel G, Czjzek M, Henrissat B, Brumer H.
984 2019. A subfamily roadmap of the evolutionarily diverse glycoside hydrolase
985 family 16 (GH16). J Biol Chem 294:15973–15986.
986 61. Tuveng TR, Arntzen MØ, Bengtsson O, Gardner JG, Vaaje-kolstad G, Eijsink
987 VGH. 2016. Proteomic investigation of the secretome of Cellvibrio japonicus
988 during growth on chitin. Proteomics 16:1904–1914.
989 62. Forsberg Z, Nelson CE, Dalhus B, Mekasha S, Loose JSM, Crouch LI, Røhr ÅK,
990 Gardner JG, Eijsink VGH, Vaaje-Kolstad G. 2016. Structural and functional
991 analysis of a lytic polysaccharide monooxygenase important for efficient utilization
992 of chitin in Cellvibrio japonicus. J Biol Chem 291:7300–7312.

993 63. Ye BC, Zhang Y, Yu H, Yu WB, Liu BH, Yin BC, Yin CY, Li YY, Chu J, Zhang SL.
994 2009. Time-resolved transcriptome analysis of Bacillus subtilis responding to
995 valine, glutamate, and glutamine. PLoS One 4.
996 64. Olea F, Pérez-García A, Cantón FR, Rivera ME, Cañas R, Ávila C, Cazorla FM,
997 Cánovas FM, De Vicente A. 2004. Up-regulation and localization of asparagine
998 synthetase in tomato leaves infected by the bacterial pathogen Pseudomonas
999 syringae. Plant Cell Physiol 45:770–780.
1000 65. Chubukov V, Sauer U. 2014. Environmental dependence of stationary-phase
1001 metabolism in bacillus subtilis and escherichia coli. Appl Environ Microbiol
1002 80:2901–2909.
1003 66. Sanchuki HBS, Gravina F, Rodrigues TE, Gerhardt ECM, Pedrosa FO, Souza
1004 EM, Raittz RT, Valdameri G, de Souza GA, Huergo LF. 2017. Dynamics of the
1005 Escherichia coli proteome in response to nitrogen starvation and entry into the
1006 stationary phase. Biochim Biophys Acta - Proteins Proteomics 1865:344–352.
1007 67. Nakagawa YS, Eijsink VGH, Totani K, Vaaje-Kolstad G. 2013. Conversion of α-
1008 chitin substrates with varying particle size and crystallinity reveals substrate
1009 preferences of the chitinases and lytic polysaccharide monooxygenase of Serratia
1010 marcescens. J Agric Food Chem 61:11061–11066.
1011 68. Hamre AG, Eide KB, Wold HH, Sørlie M. 2015. Activation of enzymatic chitin
1012 degradation by a lytic polysaccharide monooxygenase. Carbohydr Res 407:166–
1013 169.
1014 69. Bissaro B, Isaksen I, Vaaje-Kolstad G, Eijsink VGH, Røhr ÅK. 2018. How a Lytic
1015 Polysaccharide Monooxygenase Binds Crystalline Chitin. Biochemistry 57:1893–

1906.

70. Vaaje-Kolstad G, Horn SJ, Sørlie M, Eijsink VGH. 2013. The chitinolytic machinery of Serratia marcescens - A model system for enzymatic degradation of recalcitrant polysaccharides. FEBS J 280:3028–3049.

71. Navarro Llorens JM, Tormo A, Martínez-García E. 2010. Stationary phase in gram-negative bacteria. FEMS Microbiol Rev 34:476–495.

Figure 1. Growth analyses of *C. japonicus, C. pinensis,* and *S. marcescens* when provided MOPS minimal media supplemented with either (**A**) 1% (w/v) low melanin *H. bicolor* necromass or (**B**) 1% (w/v) high melanin *H. bicolor* necromass as the sole carbon sources. All growth experiments were completed in biological triplicate, with error bars representing standard deviations, although some are too small to be observed. Growth analyses were measured using test tubes and a spectrophotometer (Milton Roy Spec20D+). It should be noted that the growth analyses for each strain were conducted on different days and timepoints were taken at different intervals in order to best capture the growth dynamics of each strain on both substrates. Such data was overlayed on one graph for each substrate to compare growth dynamics between species.

Figure 2. Up regulated *C. pinensis* and *S. marcescens* CAZyme-encoding genes grown on glucose during exponential growth compared to stationary phase. Up regulated *C. pinensis* CAZyme-encoding genes are displayed in blue and those relating to *S. marcescens* are displayed in red. Genes which encode Carbohydrate-Binding Modules are abbreviated as CBM.

Figure 3. Changes to CAZyme-encoding gene expression during various growth phases on low melanin necromass. (**A**) Volcano plot representation of gene expression data for *C. pinensis* during exponential growth on low melanin necromass compared to glucose. (**B**) Volcano plot representation of gene expression data for *C. pinensis* grown on low melanin necromass during exponential growth compared to stationary phase. (**C**) Volcano plot representation of gene expression data for *C. pinensis* during stationary phase on

low melanin necromass compared to glucose. (**D**) Heat map showing changes in differential CAZyme gene expression in *C. pinensis*. (**E**) Volcano plot representation of gene expression data for *C. japonicus* during exponential growth on low melanin necromass compared to glucose. (**F**) Volcano plot representation of gene expression data for *C. japonicus* grown on low melanin necromass during exponential growth compared to stationary phase. (**G**) Volcano plot representation of gene expression data for *C. japonicus* during stationary phase on low melanin necromass compared to glucose. (**H**) Heat map showing changes in differential CAZyme gene expression in *C. japonicus*. (**I**) Volcano plot representation of gene expression data for *S. marcescens* during exponential growth on low melanin necromass compared to glucose. (**J**) Volcano plot representation of gene expression data for *S. marcescens* grown on low melanin necromass during exponential growth compared to stationary phase. (**K**) Volcano plot representation of gene expression data for *S. marcescens* during stationary phase on low melanin necromass compared to glucose. (**L**) Heat map showing changes in differential CAZyme gene expression in *S. marcescens*. Open grey circles in the volcano plots represent a single gene and colored symbols represent a CAZyme-encoding gene that correlates to the symbol/color provided in the legend.

Figure 4. Phenotypic microarray assay of *C. japonicus, C. pinensis,* and *S. marcescens* metabolic activity on various carbon and nitrogen sources. Panels **A**, **D**, and **G** correspond to *C. pinensis* activity. Panels **B**, **E**, and **H** correspond to *C. japonicus* activity. Panels **C**, **F**, and **I** correspond to *S. marcescens* activity. Carbon and nitrogen sources for each well are listed in **Tables S24-26** where **Table S24** corresponds to PM1 in panels

A-C, **Table S25** corresponds to PM2 in panels D-F, and **Table S26** corresponds to PM3 in panels G-I. Metabolic activity was determined using dye reduction kinetic curves from an OmniLog where activity is positively correlated with a brighter color.

Figure 5. Model of necromass decomposition by *C. pinensis, C. japonicus,* and *S. marcescens. C. pinensis* is hypothesized to be the early-stage degrader due to its growth-rate dependent expression of CAZyme-encoding genes. *C. pinensis* is also the only species among the three with mannanase-encoding genes. *C. japonicus* is the likely mid-stage degrader with presence throughout the degradation process due to its abundance of glucanase- and chitinase-encoding genes. Finally, *S. marcescens* is depicted as the late-stage degrader since it is exceptionally efficient at utilizing chitin as a carbon and nitrogen source. The model of necromass cell wall is simplified to only show the most common polysaccharides. Chitin is depicted in the chains of blue squares, glucans are shown as the blue circles, and mannans are shown in the green circles. In terms of the represented CAZymes, mannanases are pink, glucanases are red, and chitinases are brown.